Research Article | Vol. 26, No. 23 | 12 Nov 2018 | OPTICS EXPRESS 30444
Optics EXPRESS

Decay channels of gap plasmons in STM tunnel junctions

YAOQIN LU,[1] YUNTIAN CHEN,[1,2] JING XU,[1,2,5] TAO WANG,[3] AND JING-TAO LÜ[4,6]

[1]*School of Optical and Electronic Information, Huazhong University of Science and Technology, Wuhan 430074, China*
[2]*Wuhan National Laboratory of Optoelectronics, Huazhong University of Science and Technology, Wuhan 430074, China*
[3]*Institute of Materials Research and Engineering, A*STAR (Agency for Science, Technology and Research), 2 Fusionopolis Way, 08-03 Innovis, Singapore 138634, Singapore*
[4] *School of Physics, Huazhong University of Science and Technology, Wuhan 430074, China*
[5]*jing_xu@hust.edu.cn*
[6]*jtlu@hust.edu.cn*

Abstract: We study the decay of gap plasmons localized between a scanning tunneling microscope tip and metal substrate, excited by inelastic tunneling electrons. The overall excited energy from the tunneling electrons is divided into two categories in the form of resistive dissipation and electromagnetic radiation, which together can further be separated into four different channels, including SPP channel on the tip, SPP channel on the substrate, air mode channel and direct quenching channel. In this work, we study the enhancement factor, i.e. Purcell factor, of the STM tunnel junctions, which are mediated by the nearby metallic structures. We find that the gap plasmon mode is most likely to couple to the SPP channel on the tip, rather than the SPP channel on the substrate or the air mode. The direct quenching in the apex of tip also takes a considerable portion especially in high frequency region, the enhancement factor of direct quenching in the tip is much higher than the direct quenching in the substrate. We adopt four tips with different apex radii, i.e., 1 nm, 5 nm, 10 nm, 20 nm. When the apex size is small, the frequency dependent enhancement factor from the SPPs contribution has a pronounced peak at 1.55 eV, however, as the radius increases, the peak of enhancement factor in the high frequency region appears, the 1.55 eV peak becomes less dominated. This phenomenon can be attributed to the change of tip shape, in the form of mode coupling. Our results also show a relationship between the direct quenching in the substrate and in the tip. With the larger radius of apex, the ratio of these two part of energy approaches 1, which indicate that the energy distribution of direct quenching is sensitive to the shape of the tip-substrate gap.

1. Introduction

Since its invention in 1981, the scanning tunneling microscope (STM) has become one of the most powerful tools to characterize nanostructures on metal surface [1, 2]. It uses the quantum tunneling of electrons from the tip to the metal surface to 'measure' the local density of states of the metal surface or adsorbate on the surface. Meanwhile, the nano-gap between the tip and surface hosts localized plasmon modes (gap plasmon modes) that can be used to localize the electromagnetic field in nanoscale. Gimzewski *et al*. observed, for the first time that, the gap plasmon modes can be excited by tunneling electrons at high enough bias [3]. Radiative decay of these gap plasmon modes gives rise to light emission that is detected from the far field at the same side of the STM tip, coined as STM induced luminescence (STML). Afterwards, the effect of tip surface shape, gap size, dielectric environment, types of metal on the light emission properties are investigated [4–12]. The STM excited gap plasmon modes are also used to study

#337835 https://doi.org/10.1364/OE.26.030444
Journal © 2018 Received 5 Jul 2018; accepted 11 Oct 2018; published 6 Nov 2018

Optics EXPRESS

luminescence from single molecules [13–20]. Recently, the STML as a function of tip-surface distance is investigated from the tunneling to contact region both for metal-atom and molecular junctions [15, 21, 22], which shows that the STML is directly proportional to the shot-noise of the tunnel junction [15, 21–25].

Theoretical analysis of the light emission efficiency reveals that the gap plasmons are mainly excited by inelastic tunneling electrons in the gap, instead of hot-electron luminescence in the electrodes [26]. Electromagnetic simulations are also conducted to study the emission spectrum. In the early theoretical study of STML, metallic sphere is used to approximate the tip for the calculation of the plasmon emission spectrum in the far field [27–29]. The dependence of emission spectrum on the material, sphere radius, sphere-substrate distance and applied voltage was systematically studied. A more precise relationship between the tip shape and the spectrum is obtained by using a hyperbolic tip geometry which is similar to the tip used in experiments [30].

Recently, it was found that the gap plasmon modes can also excite the surface plasmon polaritons (SPPs) propagating along the metal surface [31, 32]. This provides a local, electrical way of launching SPPs in optical structures, and its applications received considerable attention [33–38]. These results suggest that the electrical excited gap plasmon modes have different decay channels such as radiative decay(STML), propagating SPPs, and possible quenching.

A natural question to ask is how much of the energy is transferred into different decay channels. This is important for engineering the energy ratio among different channels [39] and for improving the efficiency of STML. As far as we know, this question has not received enough attention yet. In this work, we try to answer this question from classical electromagnetic simulation by providing the enhancement factor of each energy channel.

The paper is organized as follows: In Section 2, we present the geometric setting for the decay of gap plasmons experiments and build the light emission model based on the point dipole approximation of the tunnel junction to simulate it. We further classify these decay channels with particular emphasis on separating the non-radiative quenching from the total resistive dissipation, which is usually difficult from perspective of classical electromagnetism. In Section 3, the numerical results are given and analyzed, showing that the major decay energy is distributed into the SPPs on the tip surface, and analyze the influence of the apex-radius on the enhancement factor. Finally, Section 4 concludes the paper.

2. Geometries of STM junction and decay channels

2.1. Nanoplasmonic structures used in STM luminescence

Figure 1 (a) shows the structure considered in this work, with a metallic tip positioned right above a metallic surface. The geometric properties of the tip is depicted in Fig. 1 (b). The apex has a circle shape and the radius is r. Although some efficient methods are proposed in the literature to take into account the quantum effects [40–42], we follow a classical electrodynamics simulation here. The energy source is approximated by an electrical dipole located between the tip and surface (red dot in Fig. 1 (a)). Considering the rotation symmetry of the structure, a two-dimension (2D) rotational model is adopted, and the electric dipole is implemented as a magnetic current loop with tiny radius, i.e., 0.1 nm, with the work wavelength ranging from 350 nm to 1250 nm, photon energy ranging from 1 eV to 3.5 eV.

A snapshot of the emitted electromagnetic radiation in the reduced 2D plane is presented in Fig. 1 (c). We have used the parameters of silver [43] in the simulation. The cone angle of the tip is 15 degrees. The shape of the apex also has significant impact on the spectrum. We use the sphere to represent the apex geometry used in experiment as sketched in Fig. 1 (b) when r is the radius of apex. In our model, the r is chosen to be 1 nm, 5 nm, 10 nm, 20 nm and the distance between the tip and the substrate is 1 nm.

Optics EXPRESS

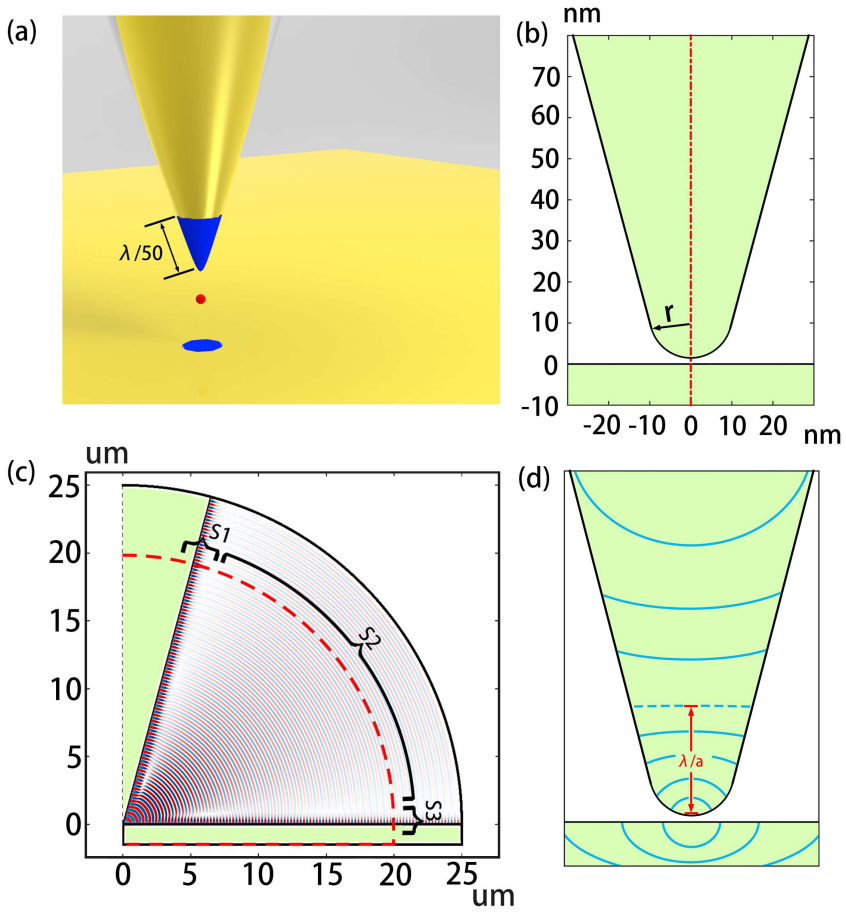

Fig. 1. (a) A three dimensional model of STM structure. Blue areas represent the direct quenching, the generatrix is about $\lambda/50$. (b) The sketch of the silver tip apex, the apex is approximated as a circle with a radius r. (c) The 2D plane of the STM structure and the radiative modes pattern. S1 and S3 are used to collect the energy of SPPs, while S2 is used to collect the energy of air mode. We integrate the energy of the SPPs modes and the air mode at a distance of 40 wavelengths away from the tip apex, while this figure is plotted at the 500 nm-wavelength (d) The sketch of the resistive dissipation contours in the area near the source. As the resistive dissipation can be attributed to both the direct quenching and the propagation loss of SPPs, we define a separation line (the dash line) to separate the areas of direct quenching and propagation losses of SPPs. The contours which are concentric to the apex are allocated to direct quenching. The contours that are much far away from the apex tend to be parallel to the tip surface, indicating the dominating effect from the propagation losses of SPPs. The height of the direct quenching area is approximately wavelength/50 for all the wavelengths.

2.2. *Decay channels of gap plasmons excited in STM junctions*

Given a volume V with its surface ∂V, the Poynting theorem states that the time rate of electromagnetic energy change within V plus the net power flowing out of V through ∂V is equal

Optics EXPRESS

to the negative of total work done on the charges within V. Here, we consider electromagnetic waves with time harmonic oscillations, thus the time rate of electromagnetic energy change within V vanishes, leading to the reduced energy conversation law, given as follows,

$$-\int_V \boldsymbol{J}\cdot\boldsymbol{E}\,dV = \oiint_{\partial V} \boldsymbol{E}\times\boldsymbol{H}\cdot d\boldsymbol{A}. \tag{1}$$

In Eq. (1), the total current density term $\boldsymbol{J}$ can be split into two terms ($\boldsymbol{J} = \boldsymbol{J}_s + \boldsymbol{J}_c$), i.e., the source current density term $\boldsymbol{J}_s$ and the polarization current density term $\boldsymbol{J}_c = \frac{d[(\epsilon_r-1)\epsilon_0\boldsymbol{E}]}{dt}$. The source current density term measures the total external work done on the electrons to generate the electromagnetic radiation, whereas the polarization current density term measures the dissipation rate into the resistive dissipation due to material losses. Indeed, in our setting the source current density term $\boldsymbol{J}_s$ corresponds to the electron tunneling between the tip and the substrate, i.e., the source of generated electromagnetic energy, while the polarization current density $\boldsymbol{J}_c$ is the energy sink of the electromagnetic radiation.

The volume V considered here corresponds to the region by rotating the area marked by red dash line along the radial direction, as shown in Fig. 1 (c), which contains the STM tunnel junction. The closed surface ∂V associated with V can be divided into four parts, i.e., $\partial V = S_1 + S_2 + S_3 + S_r$. The net energy flowing through S_1 and S_3 are the SPP channels propagating along the tip and the substrate respectively, and the photons flowing through S_2 are considered as the air mode. S_r is the rest surface of ∂V and none of energy flows through it. Since only the metals have the material losses, the resistive dissipation that absorbs energy from the electromagnetic radiation is exclusively from metals, which can be further separated into direct quenching and the propagation losses of SPPs. The direct quenching is a kind of nonradiative loss, i.e. the resistive dissipation of the electrons in the metal [44–48]. The direct quenching occurs locally, as marked as the small blue areas on the tip and the substrate in Fig. 1 (a). In contrast, the resistive dissipation from the propagation losses occurs non-locally, as long as the field amplitude of propagating SPP mode is large enough to generate heat or hot holes inside the metals. The difference between the two dissipation mechanisms of the electromagnetic radiation will be discussed and used to separate the direct quenching from the total dissipation.

There are four decay channel of gap plasmons during the electrons tunneling across the STM junction as tabulated in Tab. 1. The first one is the free propagating photons coined as the air mode channel, which is generated by the tunnel junctions and radiated into free space. Secondly, part of power from the oscillating dipole is transfered into resistive dissipation around the local area as indicated by the small blue areas on the tip and the substrate in Fig. 1 (a). This is called the direct quenching channel. Thirdly, there are two SPP channels that funnel the electromagnetic radiation along the metal-air interface, which are coined as the tip and substrate SPP channels in the following part of this paper. The tip (substrate) SPPs propagate along the metal-air interface in the tip (substrate). Their field amplitudes decay due to the propagation losses, which eventually generates resistive dissipation. In summary, the direct quenching is indicated by the small blue areas in Fig. 1 (a), the air mode is indicated by integrated power flux over the surface area S_2 shown in Fig. 1 (c) while the tip (substrate) SPPs energy is the sum of integrated power flux over S_1 (S_3) and the propagation losses in the tip (substrate), the distance we detect and integrate the energy of SPPs and the air mode is 40 wavelengths away from the source.

The Purcell factor has been routinely used to reveal the impact of plasmonic structures to light emission of various emitters. In the non-enhancement case, a dipole is positioned in the vacuum, and the energy radiated by this emitter is acquired firstly. Thus, we examine the enhancement factor, i.e., the Purcell factor, instead of the emitted power of each channel during the plasmon excitation process in STM tunnel junctions in the following. The enhancement factor equals to the ratio between the total emitted power from the emitter (the tunneling electron generating current that radiates light, seen as our emitter) and vacuum emission rate by the same emitter,

Optics EXPRESS

Table 1. Four decay channels

Four channels	Energy form	Mode properties
Air mode	Free space photons	The propagating photons in the free spaces
Direct Quenching	Heat resistance	The direct quenching in the apex of tip, which exists in the very small area, such as 1/50 wavelength away from the source due to the apex structure
SPPs on the tip	Surface plasmon polaritons	The bound surface plasmon propagating along the surface of tip, which takes the majority of the radiated energy.
SPPs on the substrate	Surface plasmon polaritons	The bound surface plasmon propagating along the surface of substrate.

i.e., without plasmonic structures. Practically, the emitter is implemented with current loop in our numerical model. In quantum electromagnetic dynamics, the total emitted power can be decomposed into various modal contents. Accordingly, the overall enhancement factor can also be divided into various modal content, which are essentially the four decay channels tabulated in Tab. 1 in our case.

2.3. Extraction of direct quenching from total resistive dissipation

In classical electromagnetism, it is not trivial to distinguish direct quenching from the propagation losses of the SPP modes in the vicinity of the tunnel junction, since both of them yield the same type of resistive dissipation, i.e, heating. The quantitative assessment of the light emission that are funneled into different channels need to be acquired. The reason that we numerically measure the integrated Poynting vectors 40 wavelengths away from the tunnel junction (see Fig. 1 (c)) is to avoid the overlap of SPPs and the air mode. To estimate the original power of SPPs excited by the tunneling electrons directly, we need to add up the resistive dissipation in metal caused by SPPs propagation. However, we have mentioned that in the vicinity of the tunnel junction, there exists direct quenching which is also kind of resistive dissipation. Here comes the question of how to separate the resistive dissipation caused by inelastic tunneling electrons and SPPs.

In this work, the separation of the direct quenching from the total resistive dissipation at the apex and the substrate are treated differently. As to the apex, the method is to set up a separation line of the tip, marked as blue dash line in Fig. 1 (d). For the direct quenching is extreme large in the tiny part of the apex and decreases dramatically in a further place, we assume it only exists in the area surrounded by the separation line in the apex, outside this area the resistive dissipation is only attributed to SPPs propagation. This separation line is derived from the contours of resistive dissipation values in the apex, which represent the attenuation characteristics of resistive dissipation. From the analysis of the resistive dissipation contours, we can find that the contours below the dash line (the contour parallel to the substrate surface) are concentric to the apex, in contrast, the contours above the dash line tend to be parallel to the surface of the tip as shown in Fig. 1 (d). It means the resistive dissipation caused by the SPPs is dominant in the area away from the tip apex, and the resistive dissipation below the dash line is attributed to the direct quenching. We find the separation distance shown in Fig. 1 (a) can be set to 1/50 of the wavelength, which turns out to a good approximation for all wavelengths in this model.

Optics EXPRESS

As to the substrate, the aforementioned method does not apply, since there is no clear separation line evident from the contour plot of the resistive dissipation shown in Fig. 1 (d). The overlap of direct quenching and propagation losses mainly appears in the vicinity of the tunnel junction. Then we introduce the theoretical SPP propagation formula, from which we prove that the ratio of the propagation loss in any two particular parts is equal between the Comsol model and the theoretical model. Thus the extraction of propagation losses in the near-source area can be achieved by multiplying the propagation losses in the far-source area by a certain ratio. As for the near-source area, we assume that all the direct quenching is included in this area. We define the radius of it as aλ in propagation direction while the center is the position of source. As for the far-source area, the resistive dissipation in this area exclusively originates from the propagation losses of SPPs and can be easily obtained from our numerical model, we set it as the 41thλ area. The ratio can be calculated from the semi-analytical formulation of the cylindrical SPPs provided by Søndergaard [49] for a dipole emitter oriented along z-axis,

$$Q = \pi\omega\epsilon_0 \int_{0(40\lambda)}^{a\lambda(41\lambda)} d\rho \int_{-\lambda}^{0} dz \rho \, \mathrm{Im}\left[\epsilon_r \left(E_\rho E_\rho^* + E_z E_z^*\right)\right]. \tag{2}$$

Based on Eq. (2), one is able to obtain the ratio between the propagation losses in the near-source area and that from the 41th λ area. The ϵ_r is the dielectric function of the metallic substrate, and see E_ρ and E_z in Appendix A. Since the exact dissipation of the propagation losses in the 41th λ area is known, one could immediately calculate the resistive dissipation from the propagation losses in the near-source area. As such, one could extract the direct quenching by subtracting the resistive dissipation of propagation losses from the total dissipation. Although the direct quenching only exists in the vicinity of the tunnel junctions, to make sure that we collect all the direct quenching, we set the radius of near-source as 7λ, which is definitely beyond the theoretical existence area of direct quenching. We have proved that the direct quenching in the substrate reaches to a constant while we detect the direct quenching in the area outside the near-source area at the wavelength of 500 nm. There is a systematic error need to be mentioned that the the propagation losses collected in the far-source area may be influenced by the noise. For the high frequency region, this may be more possible to happen due to the high decay rate of the SPPs.

3. Results

3.1. Overall analysis of decay channels

We proceed to discuss the calculated results based on the aforementioned model and to classify the energy transfer in the STM junction. The tunneling electrons can be seen as the emitters, modeled by a magnetic current loop. There are two approaches to obtain the total emitted power according to the Poynting theorem: one is to integrate the Poynting vector over a closed surface surrounding the emitter, the other is to integrate the tangential component of magnetic field along the circle with the magnetic current. As a self-benchmark, we carry out the two different procedures to obtain the total emitted power. Indeed, the two approaches yield exactly the same emission power.

We take the apexes with 1 nm, 5 nm, 10 nm, 20 nm radius size as examples to illustrate the enhancement factors of the structure used in the decay process of gap plasmons. In Fig. 2, the four curves in each plot represents the enhancement factor of overall energy radiated by the source, the total power flowing into the two SPP channels, the direct quenching channel (the sum of it in the substrate and the tip), and the air mode channel, respectively. In Fig.2 (a), the sum of SPP channels takes a dominant part of the source energy. It has a similar lineshape with the total power, sharing the same peak, which is located at the photon energy of 1.55 eV. Due to the cutoff frequency of SPP modes propagating along the interface, the SPPs energy decreases to

Optics EXPRESS

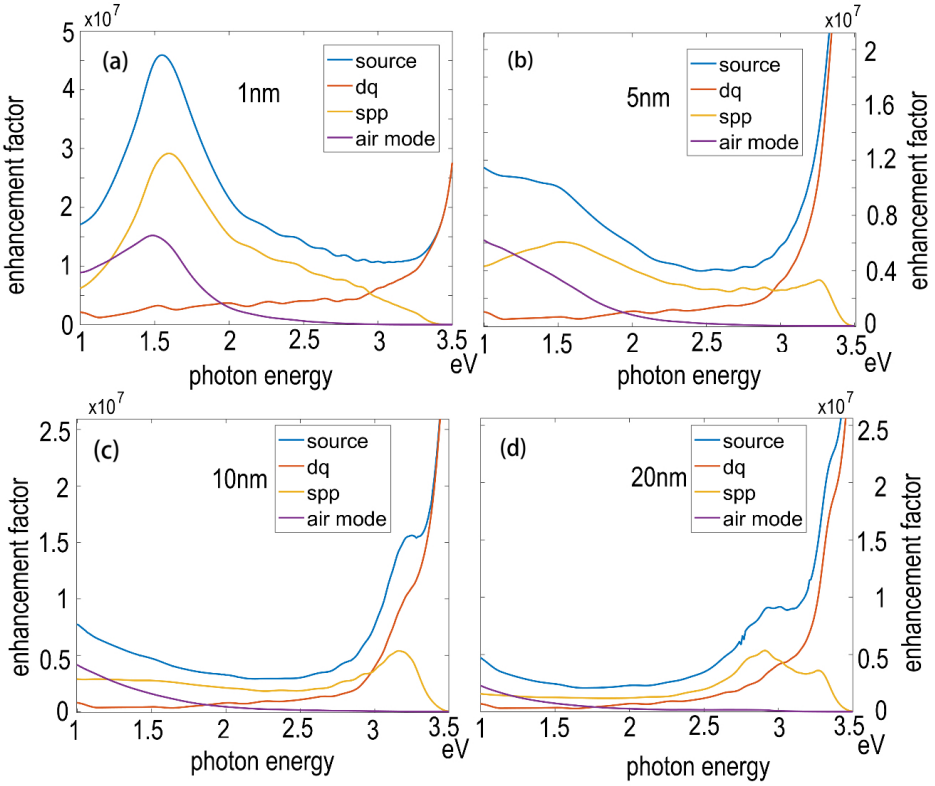

Fig. 2. (a) The enhancement factor of total power (blue) and its distribution into different channels as a function of photon energy when the radius of apex is 1 nm. The red, yellow, purple curves represent the enhancement factor of energy goes into the SPPs, direct quenching and the air mode channels, respectively. The SPPs and direct quenching (DQ) include both tip and substrate contributions. (b) (c) (d) represent the results which adopt the tip with 5 nm, 10 nm, 20 nm radius apex.

zero when the photon energy reaches 3.5 eV. As for the air mode with peak at 1.55 eV, there is a significant difference between the low frequency region and the high frequency region. The emission power into the air mode is almost zero in the high frequency region. In consistency with the experiment, the air mode is detected in the far field [22], which has approximately the same peak position. The direct quenching channel in this model has also strong frequency dependence, which dominates the high frequency region. When the frequency decreases, the direct quenching decreases monotonously.

In Fig. 2 (b)-(d), we plot the enhancement factors for the 5 nm, 10 nm, 20 nm radius apex structures, respectively, which show a few relevant features for the enhancement factors for a flatter tip apex (larger radius). Firstly, the significant losses of the SPPs mode in the low frequency region give rise to the gradual decay of the peaked enhancement factor at 1.55 eV. As for larger radius, the peaks become broader. Secondly, the enhancement factor of the air mode drops significantly. In contrast, the enhancement factor of the sum of direct quenching stays approximately unchanged for the variation of the apex radii.

Presently, the SPPs of metallic tip and substrate are considered as different channels, while the direct quenching in these two places is considered as one channel. In the following, see Fig. 3 and 4, we continue to discuss the different role of the metallic tip and substrate in this case,

Optics EXPRESS

considering the decay energy into separated SPP channels and direct quenching channels at either the tip apex or the substrate.

3.2. Emission into two SPPs channels

Figure 3 illustrates the emission into SPP channels occurring at the tip apex and the substrate. The four panels in Fig. 3 depict four different tips with different apex sizes. Apparently, the apex size has a strong impact to the emission spectrum of the two SPPs channels. As shown in Fig. 3 (a) , the enhancement factors of the two SPPs channels have the only peak in the photon energy of 1.55 eV, and share the same peak position. In contrast, we can find that there appears a peak in the high frequency region, i.e. 3.4 eV, in Fig. 3 (b). Meanwhile, the peak on the photon energy of 1.55 eV becomes less visible. We attribute this to the blue shift of such resonance for larger tip radius apex. Consistently, Fig. 3 (c)-(d) also show the same trend in terms of the emission resonance shift as the tip radius varies. One also notes that the peak value of the emission enhancement drops and the peak frequency shifts toward high frequency. This statement also applies to the SPPs emission spectrum associated with the substrate channels.

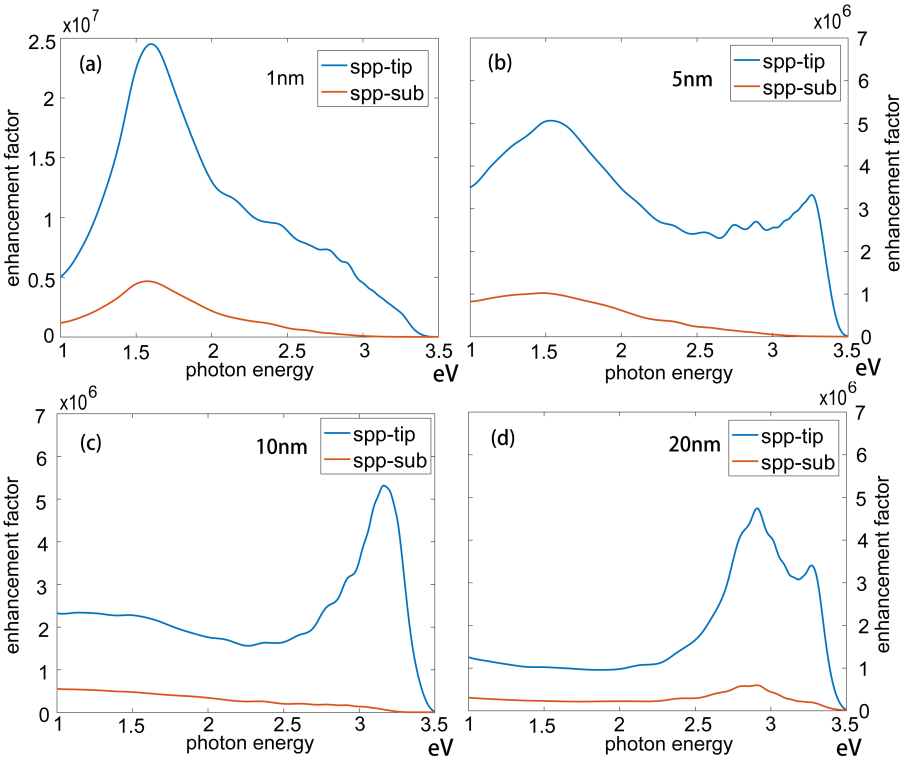

Fig. 3. (a) The enhancement factors of SPPs in tip surface and substrate surface as a function of photon energy when the radius of apex is 1 nm. (b)-(d) represent the results with tip radius being 5 nm, 10 nm, 20 nm. The two peaks with the 1.55 eV and 3.3 eV photon energy change when the apex radius increases.

The overall analysis of the four figures indicates that the enhancement factor of SPPs on the tip is much larger than it on the substrate. In consistency with the results from Fig. 2, most of the emission are funneled into the SPPs channel on the tip. Evidently, sharper apex structures give rise to larger portion of emission to tip channel, compared to that of substrate channel, which can

Optics EXPRESS

be treated as a tip with 180 degrees-cone angle. In the high frequency region, the enhancement factor drops dramatically when the frequency increases due to the cutoff frequency of SPPs. On the opposite, in the low frequency region, the changes are smooth and there appears a broader spectrum even if the peak disappears.

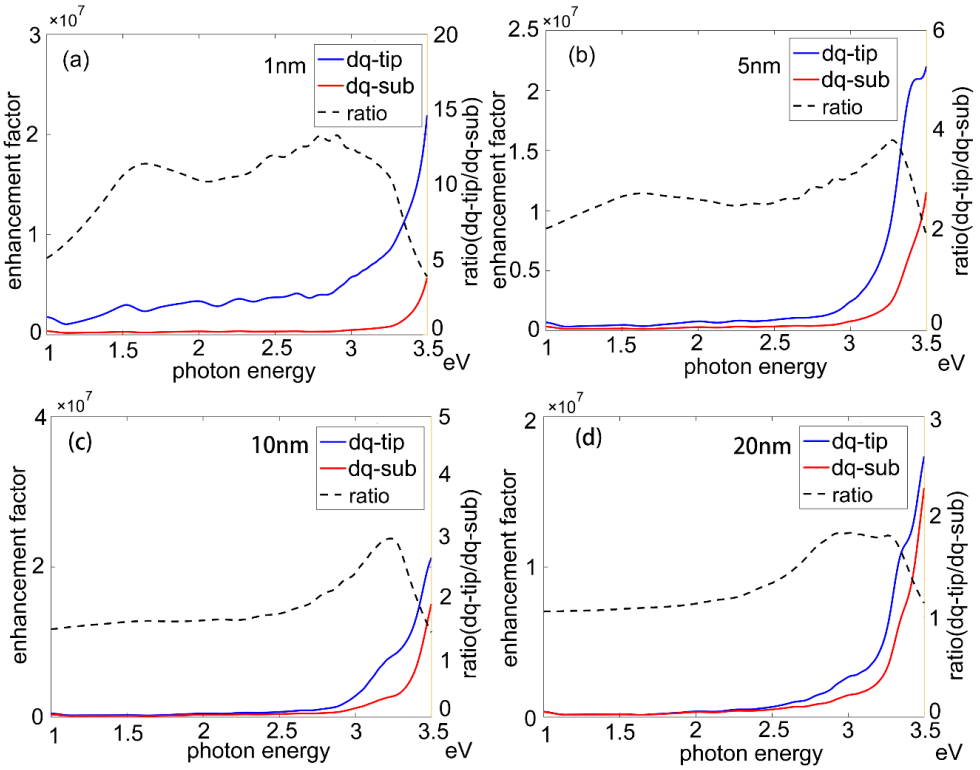

Fig. 4. (a) The enhancement factor of direct quenching in tip surface and substrate surface as a function of photon energy when the radius of apex is 1nm; (b), (c), (d) represent the results with 5nm, 10nm, 20nm tip radius.

3.3. *Direct quenching*

Figure 4 represents the enhancement factors of direct quenching associated with tip channel and substrate channel. In Fig. 4, we find that the direct quenching in the tip is much larger than that of the substrate. It increases dramatically and monotonously as the frequency increases. The sums of direct quenching from the tip channel and substrate channel remain approximately same while the radii change, in consistent with results from Fig. 2. The high value of direct quenching in the high frequency region indicates that direct quenching dominates the emission process as the photon energy is larger than 3 eV.

For larger tip radius, the emission spectrum of direct quenching in the tip channels resembles to that of the substrate channel. This is due to the fact that the surface of substrate can be treated as the arc with the infinite radius as we mentioned in section 3.2. The large tip radius behaves more like the substrate in geometry. Thus the direct quenching in these two sides tends to be identical. This can be verified by the ratio of the two curve, plotted as dot line in Fig. 4, which decreases for larger radius. Evidently, the ratio is less than 2 for 20 nm radius, while the ratio is approximately 15 for 1 nm tip radius, see Fig. 4 (a) and (d). This comparison can lead us to

Optics EXPRESS

conclude that the emission distribution of these two quenching channel is sensitive to the tip shape.

4. Conclusion

In summary, we studied the energy transfer into four different channels in the decay of gap plasmons and presented the enhancement factors of each channel. Our main result is that, the majority of the gap plasmons excited in STM junction is transferred into SPP mode on the surface of the tip. The direct quenching in the apex of the tip also takes a large part in the high frequency region. These two channels take most of the energy away, so that the energy that can be collected and utilized in the air mode and SPPs along the substrate surface is only a small portion of the total energy. The size of apex influences the SPPs dramatically. With the increase of apex radius, the peak in the low frequency region, i.e. 1.55 eV becomes less visible, and the modes in the high frequency appear. As for the direct quenching, it increases when the photon energy increases. With the increase of apex radius, the enhancement factor curve of the direct quenching in tip and in substrate become similar because of the resemblance of the flatter apex and substrate.

Appendix A: Electrical field inside the metallic region of the propagating cylindrical SPPs along metal-air interface

The electric field of SPP mode generated by an electric dipole emitter (located at $\boldsymbol{r}_0$ on z-axis) with the dipole moment being $\boldsymbol{p}$ can be given by $\boldsymbol{E}(\rho,\varphi,z) = i\omega_0\mu_0\bar{\boldsymbol{G}}_{SPP}(\boldsymbol{r},\boldsymbol{r}_0)\boldsymbol{p}\delta(\boldsymbol{r}-\boldsymbol{r}_0)$, and the SPP contribution to the Dyadic Green's function, i.e., $\bar{\boldsymbol{G}}_{SPP}(\boldsymbol{r},\boldsymbol{r}')$, reads

$$\bar{\boldsymbol{G}}_{SPP}(\boldsymbol{r},\boldsymbol{r}') = \int_0^\infty \frac{b_1^2\kappa_\rho^2 e^{b_2\kappa_\rho(z+z')}}{a(k_{SPP}^2-\kappa_\rho^2)}d\kappa_\rho \begin{pmatrix} -J_0''(\kappa_\rho\rho) & 0 & -b_1 J_0'(\kappa_\rho\rho) \\ 0 & -\frac{J_0'(\kappa_\rho\rho)}{\kappa_\rho\rho} & 0 \\ b_1 J_0'(\kappa_\rho\rho) & 0 & {b_1}^2 J_0(\kappa_\rho\rho) \end{pmatrix}, \tag{3}$$

where κ_ρ is the amplitude of the in-plane wave vector, while $a = \pi\sqrt{\epsilon_1(-\epsilon_2)}\left(1-\frac{{\epsilon_1}^2}{{\epsilon_2}^2}\right)\frac{\epsilon_1+\epsilon_2}{\epsilon_1\epsilon_2}$, $b_1 = -\sqrt{\epsilon_1/(-\epsilon_2)}$ and $b_2 = \sqrt{(-\epsilon_2)/\epsilon_1}$, and ϵ_1 (ϵ_2) is dielectric constant of air (metal). The J_1/J_0 is the first/zero order Bessel function, k_{SPP} is the wave number of SPPs. For an electric dipole emitter (the magnitude of its dipole moment $\boldsymbol{\mu}$ is 1) orientated along z-axis, i.e., $\boldsymbol{\mu} = [0,0,1]^T$, the electric field in the cylindrical coordinates can be calculated from Eq. (3) as follows,

$$\boldsymbol{E}(\rho,\varphi,z) = \int_0^\infty \frac{b_1^3\kappa_\rho^2 e^{b_2\kappa_\rho(z+z')}}{a(k_{SPP}^2-\kappa_\rho^2)}d\kappa_\rho \left(J_1(\kappa_\rho\rho)\boldsymbol{e}_\rho + b_1 J_0(\kappa_\rho\rho)\boldsymbol{e}_z\right). \tag{4}$$

Funding

Natural National Science Foundation (NSFC) (11874026, 21873033, 61775063); Fundamental Research Funds for the Central Universities (HUST) (2017KFYXJJ027); National Key Research and Development Program of China (2017YFA0305200).

Acknowledgments

We thank X. W. Chen for helpful discussions. J.T. Lv is supported by Program for HUST Academic Frontier Youth Team.

Optics EXPRESS

References

1. G. Binnig, H. Rohrer, Ch. Gerber, and E. Weibel, "Tunneling through a controllable vacuum gap," Appl. Phys. Lett. **40**(2), 178-180 (1982).
2. G. Binnig, H. Rohrer, Ch. Gerber, and E. Weibel, "Surface studies by scanning tunneling microscopy," Phys. Rev. Lett. **49**(1), 57-61 (1982).
3. J. K. Gimzewski, B. Reihl, J. H. Coomb, and R. R. Schlittler, "Photon emission with the scanning tunneling microscope," Z. Phys. B **72**(4), 497-501 (1988).
4. R. Berndt, J. K. Gimzewski, and P. Johansson, "Inelastic tunneling excitation of tip-induced plasmon modes on noble-metal surfaces," Phys. Rev. Lett. **67**(27), 3796-3799 (1991).
5. R. Berndt, J. K. Gimzewski, and P. Johansson, "Electromagnetic interactions of metallic objects in nanometer proximity," Phys. Rev. Lett. **71**(21), 3493-3496 (1993).
6. R. Berndt, R. Gaisch, J. K. Gimzewski, B. Reihl, R. R. Schlittler, W. D. Schneider, and M. Tschudy, "Photon emission at molecular resolution induced by a scanning tunneling microscope," Science **262**(5138), 1425-1427 (1993).
7. C. Chen, C. A. Bobisch, and W. Ho, "Visualization of Fermi's golden rule through imaging of light emission from atomic silver chains," Science **325**(5943), 981-985 (2009).
8. A. Yu, S. Li, G. Czap, and W. Ho, "Tunneling-electron-induced light emission from single gold nanoclusters," Nano Lett. **16**(9), 5433-5436 (2016).
9. P. Chen, W. Wang, N. Lin, and S. Du, "Manipulating photon emission efficiency with local electronic states in a tunneling gap," Opt. Express **22**(7), 8234-8242 (2014).
10. N. Nilius, N. Ernst, and H.-J. Freund, "Photon emission spectroscopy of individual oxide-supported silver clusters in a scanning tunneling microscope," Phys. Rev. Lett. **84**(17), 3994-3997 (2000).
11. S. Ushioda, "Scanning tunneling microscope (STM) light emission spectroscopy of surface nanostructures," J. Electron. Spectrosc. Relat. Phenom. **109**(1-2), 169-181 (2000).
12. R. Berndt, *Photon Emission from the Scanning Tunneling Microscope* (Springer-Verlag, Berlin Heideberg, 1998).
13. X. H. Qiu, G. V. Nazin, and W. Ho, "Vibrationally resolved fluorescence excited with submolecular precision," Science **299**(5606), 542-546 (2003).
14. Z.-C. Dong, X.-L. Guo, A. S. Trifonov, P. S. Dorozhkin, K. Miki, K. Kimura, S. Yokoyama, and S. Mashiko, "Vibrationally resolved fluorescence from organic molecules near metal surfaces in a scanning tunneling microscope," Phys. Rev. Lett. **92**, 086801 (2004).
15. N. L. Schneider, J. T. Lü, M. Brandbyge, and R. Berndt, "Light emission probing quantum shot noise and charge fluctuations at a biased molecular junction," Phys. Rev. Lett. **109**, 186601 (2012).
16. T. Lutz, C. Große, C. Dette, C. A. Kabakchiev, F. Schramm, M. Ruben, R. Gutzler, K. Kuhnke, U. Schlickum, and K. Kern, "Molecular orbital gates for plasmon excitation," Nano Lett. **13**(6), 2846-2850 (2013).
17. H. Imada, K. Miwa, M. Imai-Imada, S. Kawahara, K. Kimura, and Y. Kim, "Real-space investigation of energy transfer in heterogeneous molecular dimers," Nature **538**(7625), 364-367 (2016).
18. H. Imada, K. Miwa, M. Imai-Imada, S. Kawahara, K. Kimura, and Y. Kim, "Single-molecule investigation of energy dynamics in a coupled plasmon-exciton system," Phys. Rev. Lett. **119**, 013901 (2017).
19. Y. Zhang, Y. Luo, Y. Zhang, Y.-J. Yu, Y.-M. Kuang, L. Zhang, Q.-S. Meng, Y. Luo, J.-L. Yang, Z.-C. Dong, and J.-G. Hou, "Visualizing coherent intermolecular dipole-dipole coupling in real space," Nature, **531**(7596), 623-627 (2016).
20. Y. Zhang, Q.-S. Meng, L. Zhang, Y. Luo, Y.-J. Yu, B. Yang, Y. Zhang, R. Esteban, J. Aizpurua, Y. Luo, J.-L. Yang, Z.-C. Dong, and J. G. Hou, "Sub-nanometre control of the coherent interaction between a single molecule and a plasmonic nanocavity," Nat. Comm. **8**, 15225 (2017).
21. G. Schull, N. Néel, P. Johansson, and R. Berndt, "Electron-plasmon and electron-electron interactions at a single atom contact," Phys. Rev. Lett. **102**, 057401 (2009).
22. N. L. Schneider, G. Schull, and R. Berndt, "Optical probe of quantum shot-noise reduction at a single-atom contact," Phys. Rev. Lett. **105**, 026601 (2010).
23. J. T. Lü, R. B. Christensen, and M. Brandbyge, "Light emission and finite-frequency shot noise in molecular junctions: From tunneling to contact," Phys. Rev. B **88**, 045413 (2013).
24. F. Xu, C. Holmqvist, and W. Belzig, "Overbias light emission due to higher-order quantum noise in a tunnel junction," Phys. Rev. Lett. **113**, 066801 (2014).
25. K. Kaasbjerg, and A. Nitzan, "Theory of light emission from quantum noise in plasmonic contacts: above-threshold emission from higher-order electron-plasmon scattering," Phys. Rev. Lett. **114**, 126803 (2015).
26. B. N. J. Persson, and A. Baratoff, "Theory of photon emission in electron tunneling to metallic particles," Phys. Rev. Lett. **68**(21), 3224-3227 (1992).
27. R. W. Rendell, and D. J. Scalapino, "Surface plasmons confined by microstructures on tunnel junctions," Phys. Rev. B **24**(6), 3276-3294, (1981).
28. P. Johansson, R. Monreal, and P. Apell, "Theory for light emission from a scanning tunneling microscope," Phys. Rev. B **42**(14). 9210-9213 (1990).
29. P. Johansson, "Light emission from a scanning tunneling microscope: Fully retarded calculation," Phys. Rev. B **58**(16), 10823-10834 (1998).
30. J. Aizpurua, S. P. Apell, and R. Berndt, "Role of tip shape in light emission from the scanning tunneling microscope," Phys. Rev. B **62**(3), 2065-2073 (2000).
31. T. Wang, E. Boer-Duchemin, Y. Zhang, G. Comtet, and G. Dujardin, "Excitation of propagating surface plasmons

Optics EXPRESS

with a scanning tunnelling microscope," Nanotechnology **22**, 175201 (2011).
32. P. Bharadwaj, A. Bouhelier, and L. Novotny, "Electrical excitation of surface plasmons," Phys. Rev. Lett. **106**, 226802 (2011).
33. T. Wang, G. Comtet, E. L. Moal, G. Dujardin, A. Drezet, S. Huant, and E. Boer-Duchemin, "Temporal coherence of propagating surface plasmons," Opt. Lett. **39**(23), 6679-6682 (2014).
34. S. Cao, E. L. Moal, E. Boer-Duchemin, G. Dujardin1, A. Drezet, and S. Huant, "Cylindrical vector beams of light from an electrically excited plasmonic lens," Appl. Phys. Lett. **105**, 111103 (2014).
35. T. Wang, B. Rogez, G. Comtet, E. L. Moal, W. Abidi, H. Remita, G. Dujardin, and E. Boer-Duchemin, "Scattering of electrically excited surface plasmon polaritons by gold nanoparticles studied by optical interferometry with a scanning tunneling microscope," Phys. Rev. B **92**, 045438 (2015).
36. W. Du, T. Wang, H.-S. Chu, L. Wu, R. Liu, S. Sun, W. K. Phua, L. Wang, N. Tomczak, and Ch. A. Nijhuis, "On-chip molecular electronic plasmon sources based on self-assembled monolayer tunnel junctions," Nature Photon. **10**(4), 274-280 (2016).
37. W. Du, T. Wang, H.-S. Chu, and Ch. A. Nijhuis, "Highly efficient on-chip direct electronic-plasmonic transducers," Nature Photon. **11**, 623-627 (2017).
38. N. Cazier, M. Buret, A. V. Uskov, L. Markey, J. Arocas, G. C. D. Francs, and A. Bouhelier, "Electrical excitation of waveguided surface plasmons by a light-emitting tunneling optical gap antenna, " Opt. Express **24**(4), 3873-3884 (2016).
39. F. Bigourdan, J. P. Hugonin, F. Marquier, C. Sauvan, and J. J. Greffet, "Nanoantenna for electrical generation of surface plasmon polaritons," Phys. Rev. Lett. **116**, 106803 (2016).
40. R. Esteban, A. G. Borisov, P. Nordlander, and J. Aizpurua, "Bridging quantum and classical plasmonics with a quantum-corrected model," Nat. Commun. **3**, 825 (2012).
41. W. Zhu, R. Esteban, A. G. Borisov, J. J. Baumberg, P. Nordlander, H. J. Lezec, J. Aizpurua, and K. B. Crozier, "Quantum mechanical effects in plasmonic structures with subnanometre gaps," Nat. Commun. **7**, 11495 (2016).
42. J. Kern, R. Kullock, J. Prangsma, M. Emmerling, M. Kamp, and B. Hecht, "Electrically driven optical antennas," Nature Photon. **9**, 582-586 (2015).
43. P. B. Johnson, and R. W. Christy, "Optical constants of the noble metals," Phys. Rev. B **6**(12), 4370-4379 (1972).
44. D. E. Chang, A. S. Sørensen, P. R. Hemmer, and M. D. Lukin, "Quantum Optics with Surface Plasmons," Phys. Rev. Lett. **97** 053002 (2006).
45. D. E. Chang, A. S. Sørensen, P. R. Hemmer, and M. D. Lukin, "Strong coupling of single emitters to surface plasmons," Phys. Rev. B **76** 035420 (2007).
46. Y. Chen, T. R. Nielsen, N. Gregersen, P. Lodahl, and J. Mørk, "Finite-element modeling of spontaneous emission of a quantum emitter at nanoscale proximity to plasmonic waveguides," Phys. Rev. B **81** 125431 (2010).
47. Y. Chen, N. Gregersen, T. R. Nielsen, J. Mørk and P. Lodahl, "Spontaneous decay of a single quantum dot coupled to a metallic slot waveguide in the presence of leaky plasmonic modes," Opt. Express **18**(12), 12489-12498 (2010).
48. L. Novotny and B. Hecht, *Principles of nano-optics,* (Cambridge University Press, 2006).
49. T. Søndergaard, and S. I. Bozhevolnyi, "Surface plasmon polariton scattering by a small particle placed near a metal surface: An analytical study," Phys. Rev. B **69**, 045422 (2004).